Advanced Physics Lab II

Lab Report #2

Electron Spin & Nuclear Magnetic Resonance

Group 1
Noah Horne, Luka Burduli

11/03/2025

Dr. Arnulf Materny
Dr. Faezeh Mohaghegh

We hereby declare that we (Luka Burduli and Noah Horne) are the sole authors of this lab report and have not used any sources other than those listed in the bibliography and identified as references throughout the report.

_____ _____

Contents

1 Abstract 2

2 Introduction & Theory 2

3 Setup & Experimental Procedure 9

4 Results and Data Analysis 13

5 Error Analysis 23

6 Discussion 25

7 Conclusion 26

8 Bibliography 28

References 28

1 Abstract

Electron Spin Resonance and Nuclear magnetic Resonance are phenomena which occur when an organic material with a free radical is exposed to a static magnetic field, and an orthogonally incident high frequency AC magnetic field. By nature of the high frequency in the orthogonal B-field, energy is introduced to the material, causing resonance if the frequency is such that the exact energy required to shift is given. For the investigation into ESR, the Landé g-factor of a free electron was calculated through the use of a DPPH element to be $g_J = 1.91 \pm (5.9 \cdot 10^{-3})$, and the resultant width of the magnetic field strengths δB was calculated to be $(2.47 \pm 0.4) \cdot 10^{-4}[T]$, $(2.37 \pm 0.4) \cdot 10^{-4}[T]$, $(2.19 \pm 0.4) \cdot 10^{-4}[T]$ for resonant frequencies of 50MHz, 60MHz and 70MHz respectively. Furthermore, the transition state lifetime (time taken between states) T was calculated to be $(1.27 \pm 0.222) \cdot 10^{-8}[s]$. For the analysis of NMR, the g-factor of Glycerin, Polystyrene, Teflon, and Plant Matter were determined to be 5.56 ± 0.93,5.46 ± 0.13,5.36 ± 0.5,5.68 ± 0.5 respectively. All calculated values agree with the literature to a commensurable degree.

2 Introduction & Theory

This investigation primarily focuses on the analysis of electron spin resonance (ESR) exhibited by electrons exposed to a fixed magnetic field perpendicular to a high frequency oscillating B-field, and nuclear magnetic resonance due to similarly invoked physical scenarios. To begin, the theory and general background required to perform the Electron Spin Resonance experiment will be examined.

In the context of this specific investigation, the molecular structure of f 1,1-diphenyl-2-picryl-hydrazyl (DPPH) will be exploited to more easily observe ESR phenomena in a laboratory setting under a weak fixed magnetic field strength $\vec{B}$ of no more than a few mT. By analyzing the internal magnetic fields behavior of this DPPH sample, its corresponding Landé g-factor will be calculated. The DPPH sample subject to a static magnetic field $\vec{B}_0$ is an organic compound and a relatively stable free radical. The feature of this compound that makes it an ideal candidate for the examination of ESR is its singular free valence electron present at its nitrogen bridge (presence of a free radical). Due to the molecular structure of the DPPH compound, much of the orbital motion of the valence electron is cancelled out, and the electron behaves semi-freely across the molecular lattice (Materny & Mohaghegh, 2025). This dynamic creates a very strong ESR line with a very small width due to resultant exchange narrowing.

Electron spin resonance is an advanced quantum phenomenon which takes advantage of resonance in relation to the discrete orbital potential energies of an electron orbiting a molecular structure. Electron spin resonance (ESR) is only applicable to paramagnetic materials able to absorb high-frequency radiation in an external magnetic field. When subject to a fixed magnetic field $\vec{B}_0$, the discretized electron spin states are further split due to the consequent Zeemann

effect, and allows the magnetic field of the material and/or the magnetic moment $\vec{\mu}_J$ of the paramagnetic compound to be measured very precisely (Materny & Mohaghegh, 2025) . ESR is an invaluable method of investigating molecular and crystal structures, chemical reactions and other problems in physics, chemistry, biology and medicine, still widely employed today in industry.

When an electron orbits its nucleus, while the whole molecular structure is subject to a magnetic field, a magnetic interaction occurs. This interaction involves two separate magnetic fields, the internal magnetic field of the molecule and/or nucleus, and the external static and AC B-field incident on the sample. More specifically, the molecular nucleus and the electron form a magnetic dipole, and this dipole is subject further to a fixed static B-field. As a result, this magnetic dipole (mediated by the electrons behavior) can be expressed quantitatively through a magnetic moment $\vec{\mu}$. As one may recall from quantum theory and the theory of particles, electrons orbiting a nucleus carry two principal forms of angular momentum: orbital angular momentum $\vec{L}$, and spin angular momentum $\vec{S}$. Through a combination of these two angular momentum components, the complete magnetic dipole moment $\vec{\mu}_J$ of a molecular compound can be properly described. Adapting a perspective that only looks upon the electron spin and orbital motion separately, two magnetic dipole moments emerge–one moment is induced from the intrinsic spin angular momentum of the electron $\vec{\mu}_s$, and another is induced by the orbital momentum of the electron. Focused only on the orbital angular momentum of the electron, its resultant orbital angular momentum magnetic moment $\vec{\mu}_L$ can be formulaically expressed in terms of the quantized angular momentum as:

$$\vec{\mu}_L = \frac{-e}{2m_e}\vec{L} = -\mu_B\frac{\vec{L}}{\hbar} \tag{2.1}$$

where e is the elementary charge $\approx 1.6 \cdot 10^{-19}[C]$, m_e is the mass of an electron, $\approx 9.11 \cdot 10^{-31}[kg]$, $\hbar$ is the reduced Planck constant $\hbar = \frac{h}{2\pi}$, and μ_B is the Bohr Magneton (Materny & Mohaghegh, 2025). As one can observe from the equation above, the orbital momentum magnetic moment $\vec{\mu}_L$ is quantized in units of this special quantity μ_B, the Bohr Magneton. This quantization consequently implies that the angular momentum of the electron can be correspondingly quantized in units of $\hbar$. The Bohr Magneton has units $J \cdot T^{-1}$, and can has a fixed numerical value defined by the formula:

$$\mu_B = \frac{e\hbar}{2m_e} \approx 9.274 \cdot 10^{-24}[J \cdot T^{-1}] \tag{2.2}$$

The Bohr Magneton is a common physical constant which is recurrently applied as a natural unit for the magnetic moment of an electron and is used to quantize both the orbital and spin angular momentum as first observed in equation 2.1 (Materny & Mohaghegh, 2025). Treating the angular momentum as a quantum operator on a wavefunction ψ, its components L_x, L_y, L_z, have specific eigenvalues. While the derivation of these eigenvalues is outside of the scope of this investigation, out of interest the basic mathematics is as follows. One can express $L^2 = \vec{L} \cdot \vec{L} = \vec{L}_x^2 + L_y^2 + L_z^2$ as a quantum operator which acts on a wave function ψ. Taking

L_z to be a quantum angular momentum operator which is parallel to the static B-field, its values become quantized due to the corresponding quantization of its eigenvalues when acting on the wave function. In doing so, one can observe that L_z is quantized according to:

$$L_z = m_l\hbar, \text{ where } m_l = -l, (-l+1), \ldots, (l-1), l \tag{2.3}$$

and as a result the angular momentum itself is partially quantized as $|\vec{L}| = \sqrt{l(l+1)} \cdot \hbar$, where $l \in \mathbb{N}_0$, causing the magnetic moment magnitude $|\vec{\mu}_L|$ to be quantized as well according to the equation:

$$|\vec{\mu}_L| = \mu_B\sqrt{l(l+1)} \tag{2.4}$$

So, from the discretized nature of the eigenvalues of the angular momentum quantum operator on wave function ψ of the electron it can be found by propagating this discretization through to the magnetic moment, that its magnitude $|\vec{\mu}_L|$ is also quantized, namely by $l \in \mathbb{N}_0$. Analogously, one can impose this same quantization onto the spin angular momentum $\vec{S}$, and consequently the magnetic moment due to the spin of the electron $\vec{\mu}_S$. The spin magnetic moment of an electron can be expressed very similarly to the orbital magnetic moment, only now with an additional quantization factor which arises due to the spin of the electron called the g-factor g_e.

$$\vec{\mu}_S = -g_e \cdot \mu_B \frac{\vec{S}}{\hbar} \tag{2.5}$$

This new g-factor observed in equation 2.5 is in fact present in the equation of the magnetic moment due to orbital angular momentum $\vec{L}$, however is not shown due to the fact that the Landé g-factor of an electron that has a magnetic moment solely due to orbital angular momentum $\vec{L}$ is 1, e.g. $g_L = 1$. In the case of a quantum Dirac particle with no assumed internal substructure, the spin of the particle would be $1/2$, leading to a corresponding Landé g-factor of approximately 2, $g_e = 2.002319$ (Materny & Mohaghegh, 2025). In the case of this investigation, the DPPH element used to analyze ESR has a molecular structure such that almost all orbital motion of the electrons is canceled, resulting in free electron behavior and a very diminished angular orbital momentum. As a result, most of the angular momentum of the electron in the DPPH element comes from its intrinsic spin, so the g-factor one expects to calculate during this experiment should range close to 2 due to such major spin contributions.

Similar to the quantization of the orbital magnetic moment of the semi-free electron, the spin magnetic moment of the electron is similarly quantized due to the quantization of the z-component of the spin angular momentum, for similar reasons. As a result, the spin magnetic moment $\vec{\mu}_S$ is quantized in magnitude with respect to the eigenvalues of the spin operator acting on the wave function of the corresponding electron ψ, e.g:

$$|\vec{\mu}_S| = g_e \cdot \mu_B\sqrt{s(s+1)}, \quad \because \text{(Dirac Particle)} \implies s = \frac{1}{2} \tag{2.6}$$

As aforementioned, electron spin resonance is a phenomenon specific to paramagnetic materials or organic free radicals. In materials which contain individual unpaired atoms such as the DPPH sample analyzed during this experiment, the total angular momentum $\vec{J}$ of the electrons is different from zero, and thus may be considered as the principal descriptor of the angular momentum of the quantum system, and thereby the magnetic moment which dictates the interaction of the electron and the external magnetic field.

$$\vec{J} = \vec{S} + \vec{L} \neq \vec{0} \tag{2.7}$$

As previously derived, the magnetic moment $\vec{\mu}_J$ associated with the total angular momentum $\vec{J}$ can be written out and quantized with respect to a specific g-factor called the Bohr magneton μ_B and the Landé g-factor, the major subject of this investigation. The magnetic moment and its corresponding magnitude derived by the eigenvalues of the total angular momentum operator are given as:

$$\vec{\mu}_J = -g_J \cdot \mu_B \frac{\vec{J}}{\hbar} \tag{2.8}$$

$$|\vec{\mu}_J| = g_J \cdot \mu_B \sqrt{j(j+1)} \tag{2.9}$$

In these equations, the eigenvalue of the total angular momentum $\vec{J}$ operator is defined as:

$$\vec{J}|\psi\rangle = \left[\frac{\sqrt{j(j+1)}}{\hbar}\right]|\psi\rangle \tag{2.10}$$

and as such shows up in equation 2.9 respectively where j is the total angular momentum quantum number which takes values that express themselves as the sum of the two quantum numbers which define the spin angular magnetic moment $\vec{\mu}_S$ (quantum number s) and orbital angular magnetic moment $\vec{\mu}_L$ (orbital quantum number) as $j = l \pm s$. Again, the total angular momentum magnetic moment is quantized in units of the Bohr magneton μ_B and the Landé g-factor g_J, dictated by the total angular momentum quantum number j.

When exposed to an external magnetic field $\vec{B}_0$, it is well known that any magnetic dipole which sits in this magnetic field carries a specific potential energy E, characterized by its alignment with respect to the magnetic field (Materny & Mohaghegh, 2025). The more aligned the magnetic moment $\vec{\mu}_J$ is from the B-field, the larger the respective potential energy of the particle in question. Formulaically, this energy-orientation relationship with respect to the static B-field $\vec{B}_0$ can be described in a dot product as:

$$E = -\vec{\mu}_J \cdot \vec{B}_0 \tag{2.11}$$

where $\vec{\mu}_J$ is the total angular momentum magnetic moment, and $\vec{B}_0$ is the external fixed magnetic field which warrants the resultant magnetic interaction (Materny & Mohaghegh, 2025). As previously discussed, it is known that the total angular momentum is quantized. As the to-

tal angular magnetic moment is dependent on this angular momentum, the moment $\vec{\mu}_J$ is also consequently quantized. Propagating this error further, the energy of the electron and its state is also discretely dictated by the quantization of the total angular magnetic moment $\vec{\mu}_J$, leading to the following split energy levels:

$$E = g_e \cdot \mu_B \cdot m_j \cdot B_0 \tag{2.12}$$

where m_j is defined as the total magnetic moment quantum number $m_j = -j, -j+1, \ldots, j-1, j$ where j is the aforementioned total angular momentum quantum number which takes on only values expressed as a sum of the two other quantum numbers for spin and orbital angular momentum $j = l \pm s$ (Materny & Mohaghegh, 2025).

As the energy of the electron is now quantized, the energy difference between two neighboring energy levels can be calculated and resultantly exploited to find resonance among this quantum system. Examining equation 2.12 a little closer, it is clear that the quantization is mediated by the total angular momentum quantum number m_j. As we know that $\Delta m_j = 1$ as it is defined as $m_j = -j, -j+1, \ldots, j-1, j$, it is clear then that the difference between energy levels can be given by the equation:

$$\Delta E = g_J \cdot \mu_B \cdot |\vec{B}_0| \tag{2.13}$$

where g_J is the Landé g-factor, μ_B is the Bohr magneton, and $|\vec{B}_0|$ is the magnitude of the incident external fixed magnetic field.

As the name of the phenomena 'Electron Spin Resonance' suggests, it is now necessary to achieve resonance of the magnetic field by introducing the exact energy necessary to change the state of the quantum system periodically. As the interaction which governs the potential energy of the system is purely magnetic and parallel to the z component of the angular momentum, an additional stimulatory alternating B-field $\vec{B}_1$ can be orthogonally implemented to allow for potential energy E to be introduced into the system. This orthogonally positioned variable external magnetic field $\vec{B}_1$ should be modulated at a very high frequency such that:

$$\vec{B}_1 = \vec{B}_{HF} \cdot \sin(2\pi \cdot \nu \cdot t) \tag{2.14}$$

where B_{HF} is the vector amplitude of the oscillating magnetic field, and ν is the frequency of the oscillation. As the inner argument of the $\sin$ term is scaled by 2π, this is exactly why ν represents the actual frequency of the oscillation, rather than the angular frequency, as $\omega = 2\pi f$. At high a given frequency of oscillation, the energy transmitted to the DPPH sample by the oscillating magnetic field can be given by the relativistic formula for energy in terms of frequency, e.g.:

$$E_{B_1} = hf \tag{2.15}$$

As is known from the previously established theory, the energy levels which separate different

states of the electron in the DPPH compound are split by the amount stated in formula 2.13. To achieve an ideal resonance, one should equate the energy introduced by this oscillating magnetic field $\vec{B}_1$ and the energy difference due to the quantization of the total angular momentum and the discrete values of the total angular momentum quantum number m_j. In doing so, one achieves the most important formula for this investigation.

$$h\nu = g_J \cdot \mu_B \cdot B_0 \iff \nu = \frac{g_J \cdot \mu_B}{h} \cdot B_0 \tag{2.16}$$

As one can immediately conclude from equation 2.16, a directly proportional relationship between frequency ν of variable magnetic field strength $\vec{B}_1$ is obtained. As the Bohr magneton μ_B and the Landé g-factor g_J are known, the slope of equation 2.16 can be rearranged to calculate the Landé g-factor g_j, which is exactly what is done throughout the first part of this investigation.

As previously discussed, the frequency of the AC B-field is exactly matched to resonate with the orbiting electrons. However, it is crucial to note that as this is a quantum system, there are uncertainties which must be taken into account. Specifically the fact that the energy level and the lifetime of the electron in Hilbert space do not commute as operators. For this reason, they are subject to the Heisenberg uncertainty in energy and time. This uncertainty relation is expressed below.

$$\delta E T \geq \frac{\hbar}{2} \tag{2.17}$$

Furthermore, as the energy change and intensity of the incident B-field are directly related through equation 2.13, one can substitute ΔE for the new uncertainty of E to arrive at the formula:

$$\delta E = g_J \mu_B \delta B_0 \tag{2.18}$$

where to accommodate for the δE substitution of ΔE, δB_0 is the respective half-width of the absorption line (Materny & Mohaghegh, 2025). A small issue with the construction of equation 2.18 is the reference to two virtually unmeasurable quantities. The full width half maximum of the energy is quite difficult to directly measure, and the full width half maximum of the B field is similarly difficult to measure across the sample due to its spatial variation. To solve this problem, one may take advantage of the relationship between the energy and voltage/current measured by the ESR element during the experiment. As the absorbed energy is directly related to the measured voltage, one can also associate an uncertainty to the measured voltage, and in turn, the applied current by scaling with respect to the modulate voltage and current respectively. Below is the equation which expresses this relationship:

$$\delta I = \frac{\delta U}{U_{mod}} I_{mod} \tag{2.19}$$

where δU is the half width of the absorption line expressed as a voltage, U_{mod} is the modulation voltage, and I_{mod} is the modulated current (Materny & Mohaghegh, 2025). To directly relate equation 2.19 to the B field for application to equation 2.18, the relationship between current across the Helmholtz coils and the resultant magnetic field strength must be known. Theoretically, this relationships is given as:

$$B = \mu_0 \left(\frac{4}{5}\right)^{\frac{3}{2}} \frac{n}{r} I \implies \delta B = \mu_0 \left(\frac{4}{5}\right)^{\frac{3}{2}} \frac{n}{r} \delta I \tag{2.20}$$

where I is the current across each Helmholtz coil, μ_0 is the permeability of free space $\approx 4\pi \cdot 10^{-7} mkgs^{-2}A^{-2}$, n is the number of their wrappings, and r is the radius of the coils (Materny & Mohaghegh, 2025). Using equation 2.20 in conjunction with the manually calculated FWHM of the voltage absorption line propagated through equation 2.19 to yield the uncertainty of the half width of the B field, which is what was to be calculated. Using the half width of the incident B-field and combining equations 2.18 and 2.15, one can deduce a formula relating the half width of the B-field and the lifetime of the transition state T, which can then be respectively calculated.

$$T = \frac{\hbar}{2 g_J \mu_B \delta B_0} \tag{2.21}$$

With all equations defined, the relevant information of the landé factor g_J, half width of B-field δB_0, and lifetime of transition state T can be calculated as a thorough investigation of the ESR phenomena.

As for nuclear magnetic resonance, the theory applied is quite similar to that of electron spin resonance, only that now the excitation and energy levels occur in the nucleus of an organic molecule rather than in the spin of the electrons. As one can recall from Quantum Physics, the energy levels of the nucleus are discretized as well, and due to a similar effect, can be directly influenced an external magnetic field to be precisely measured. In this experiment, nuclear magnetic resonance and its respective properties will be exploited in order to determine the Landé nuclear g-factor of 4 different organic substances: glycerin, PTFE (teflon), polystyrene, and an assorted plant leaf. Very similar to the energy levels of the electron. The discretization of the energy levels in the nucleus can be describe formulaically as:

$$E = g_{J_N} \mu_N m_{j_N} B_0, \text{ with } m_{j_N} = -j_N, -j_N + 1, \ldots, j_N - 1, j_N \tag{2.22}$$

where g_{j_N} is the nuclear g-factor, μ_N is the nuclear magneton $\approx 5.051 \cdot 10^{-27} [JT^{-1}]$, and m_{j_N} is the total magnetic moment quantum number of the nucleus, discretized as above (Materny & Mohaghegh, 2025). By applying this formula and again equating it to the frequency of the fast oscillating perpendicular B-field ν, one achieves a similar relation to determine the nuclear g-factor of the examined material.

$$\nu = \frac{g_{j_N} \mu_N}{h} B_0 \tag{2.23}$$

In the equation above, g_{j_N} is the nuclear g-factor, μ_N is the nuclear magenton $\approx 5.05 \cdot 10^{-}27[JT^1]$. By applying formula 2.23 and examining the linear relationship between the incident magnetic field strength (measured using a Hall Probe) and the frequency of the fast oscillating perpendicular b-field, the nuclear g-factor of all materials can be swiftly determined. As each nucleus has it's own g-factor, by subjecting an organic molecule to a NMR sceme, determining the g-factor of the material tells an observer the exact contributor through the comparison of literature values for molecules such as Hydrogen-1, Carbon-13, Fluorine-19, Oxygen-17 (Materny & Mohaghegh, 2025).

3 Setup & Experimental Procedure

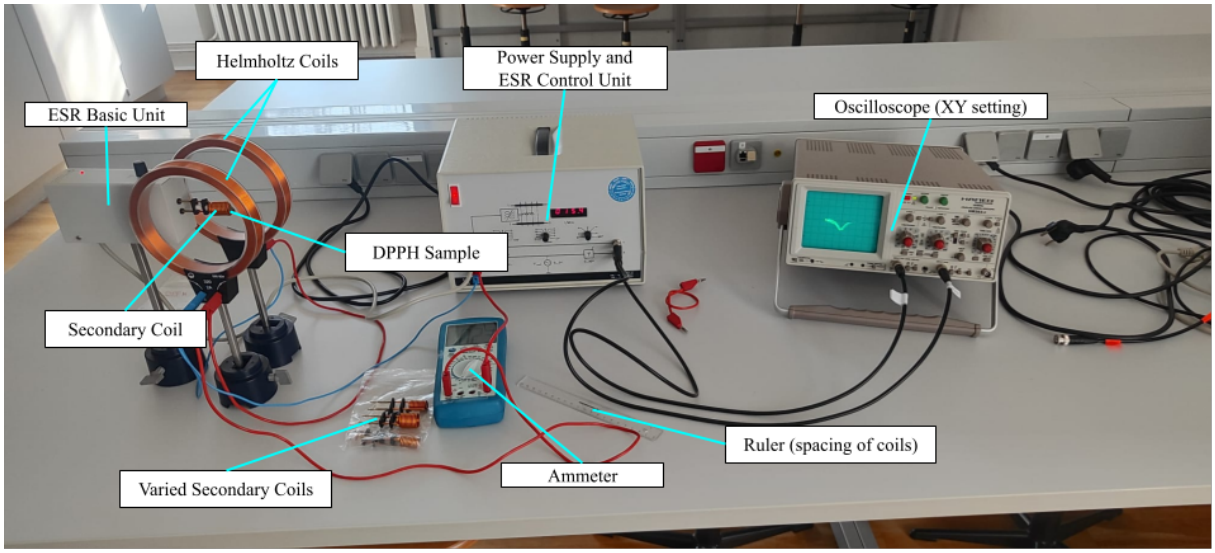

Figure 1: Annotated Setup Diagram for Electron Spin Resonance

To begin, the Helmholtz coils responsible for mediating a constant B-field across the DPPH sample were connected in parallel, and consequently in series through an ammeter running to a DC power supply as observed in figure 1. After the Helmholtz coils were in position, the ESR basic unit without the sample was positioned such that the secondary high frequency coil–that which surrounds the DPPH Sample and delivers a the high frequency ν perpendicular magnetic field B–was directly in the center of the two Helmholtz coils. To extract meaningful measurements from these instruments, an oscilloscope was connected directly to the frequency modulating power supply. The two channels of the oscilloscope corresponded to the output of the ESR basic unit, ran back through the frequency modulating power supply, and the resultant output of the ESR control unit as observed in the figure above.

For the effective electrical transportation of the high frequency signal from the ESR Control Unit to the ESR Basic Unit, a 6 pole cable was used. As is, the setup still would be unable to provide any meaningful results without the consideration and calibration of a few key features. To begin, due to the inductors used in this experiment and their setup, a time delay is introduced between the electrical signal of the high frequency oscillating b-field and the corresponding response. To account for this time-difference on the oscilloscope, the phase difference between these two signals was required to be calibrated after every measurement for accurate results. When the phase difference was aligned appropriately on a corresponding excitation frequency, the oscilloscope would display a very nice peak indicating the resonance of the electrons' energy levels in the DPPH material.

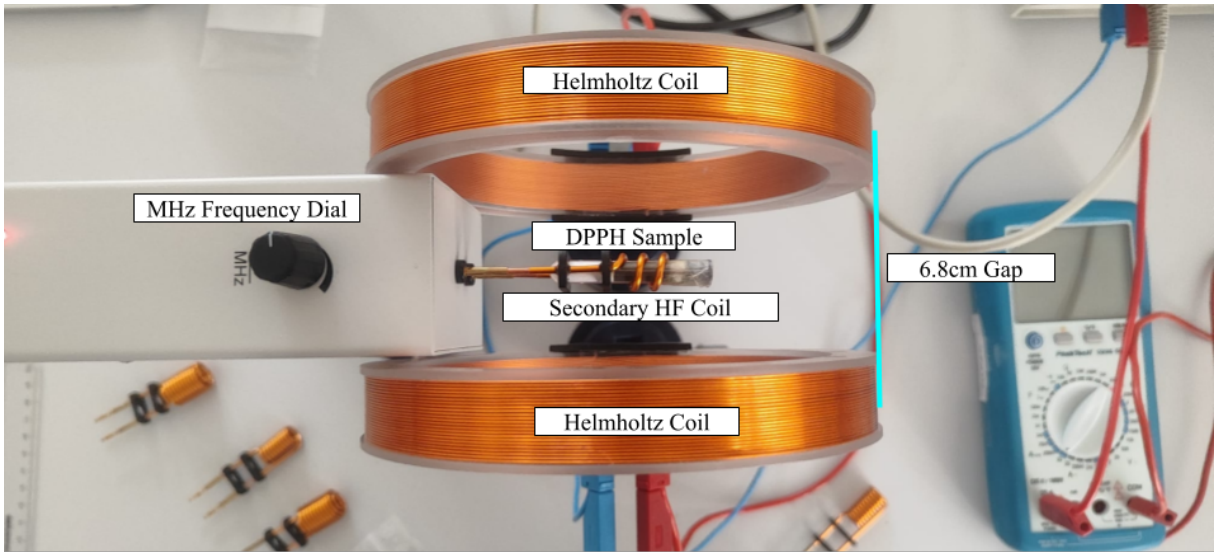

Figure 2: Top-Down Annotated Diagram of Calibrated Helmholtz Coil Setup

However as briefly aforementioned, such resonance does not occur unless the frequency of the ESR Basic Unit and its coil are perfectly aligned such that the energy given to the DPPH sample corresponds directly to its newly discretized electron energy levels. To calibrate the setup in order to ensure that the process of finding this resonant flows as seamlessly as possible, the position of the Helmholtz coils with respect to the ESR Basic unit and DPPH sample was required to be precisely set up. As one can see from figure 2, a very precise 6.8 centimeter gap between the center of the Helmholtz coils was used to ensure a uniform and theoreticaly accurate B-field current relation B-I across the DPPH Sample. Should one of the Helmholtz coils have been crooked, then the magnetic field across the sample, although small, would receive major fluctuations from the theoretical value and greatly inhibit the ability to find resonant frequencies in a timely manner. After an appropriate distance between the Helmholtz coils was found, the DPPH Sample was placed in the exact center of the two Helmholtz coils such that it lied in a position of maximum superposition between the two diametrically opposed B-Fields. By fixing

the distance between the Helmholtz coils at 6.8 centimeters and centering the DPPH samples, the simpler reproducibility of our measurements is ensured.

After the setup was complete and calibrated, the resonant frequency was measured against the fixed magnetic field strength B_0 across the DPPH sample, calculated from the current that was varied across the Helmholtz coils using equation 2.20. For lower currents across the Helmholtz coils, lower magnetic field strengths were produced, leading to lower resonant frequencies of the DPPH sample. As a result, for lower currents across the Helmholtz coils, a smaller frequency was required, and a larger secondary coil was used. As the current across the Helmholtz coils increased, and consequently the magnetic field across the DPPH sample increased, the resonant frequency of the DPPH sample rose linearly, and a smaller secondary high frequency coil had to be used to ensure the high frequency could be handled by the Copper. As one can see in figure 1, 3 different varied secondary coils were used throughout the measurement series to accommodate the higher frequencies and provide an accurate result. In data, the different coils are represented through a color scheme in the tables and graphs, as observed in section 4.

For the second aspect of the ESR investigation–the determination of the transition lifetime and half width of the magnetic field B_0–measurements of the full width half maximum of the voltage curve δU on the oscilloscope, the resonant frequency for the corresponding current, and the modulated voltage and current were taken. To calculate the full width half maximum of the voltage curve δU, image processing was used to determine the exact FWHM of the voltage peak displayed on the oscilloscope, specifically through the use of Desmos and its line drawing capabilities. The details of this method can be observed in figure 3 below.

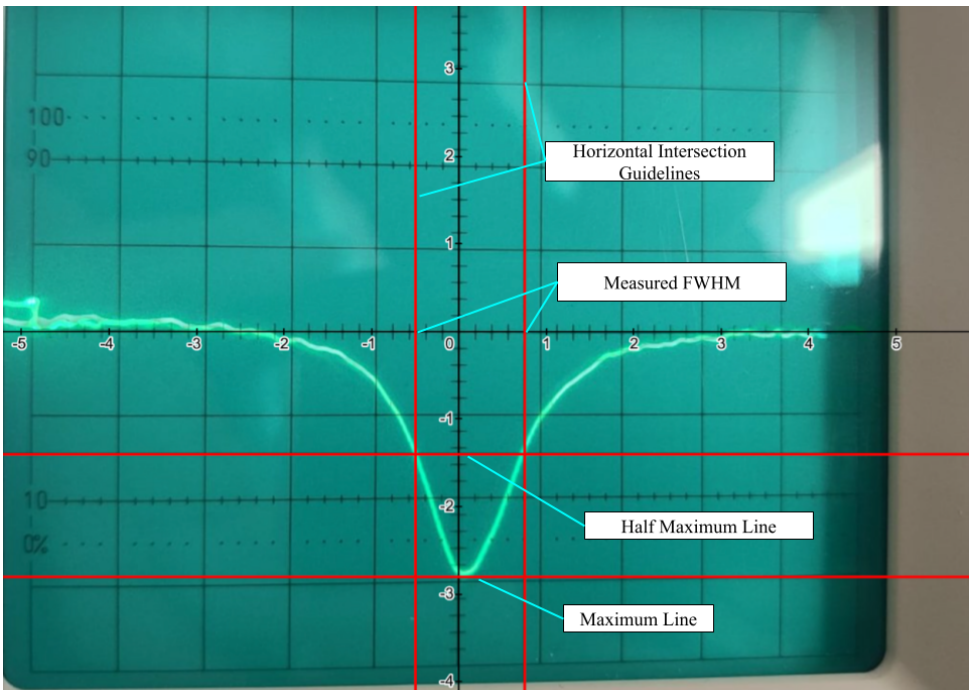

Figure 3: Sample Demonstration of Image Processing Determination of FWHM δU

The image of the peak was imported into Desmos and laid onto a cartesian plane. the origin of the oscilloscope was centered to the origin of the cartesian plane, and a red line was fit to the peak voltage of our curve. After this was done, the constant value determined for the maximum line was halved, and the corresponding horizontal line plotted. By then constructing horizontal lines marking the intersection between the curve and the half maximum line, the FWHM of the voltage curve could be measured accurately to a precision of ± 0.1V. Using the calculated value of the FWHM of the voltage, the formulas derived during the theoretical introduction 2.19, 2.20, 2.21 were applied to calculate the corresponding half width of the B-field δB_0 and consequently the transition lifetime T of the electrons in the DPPH sample. After these measurements are taken, a thorough data analysis is performed and errors are calculated.

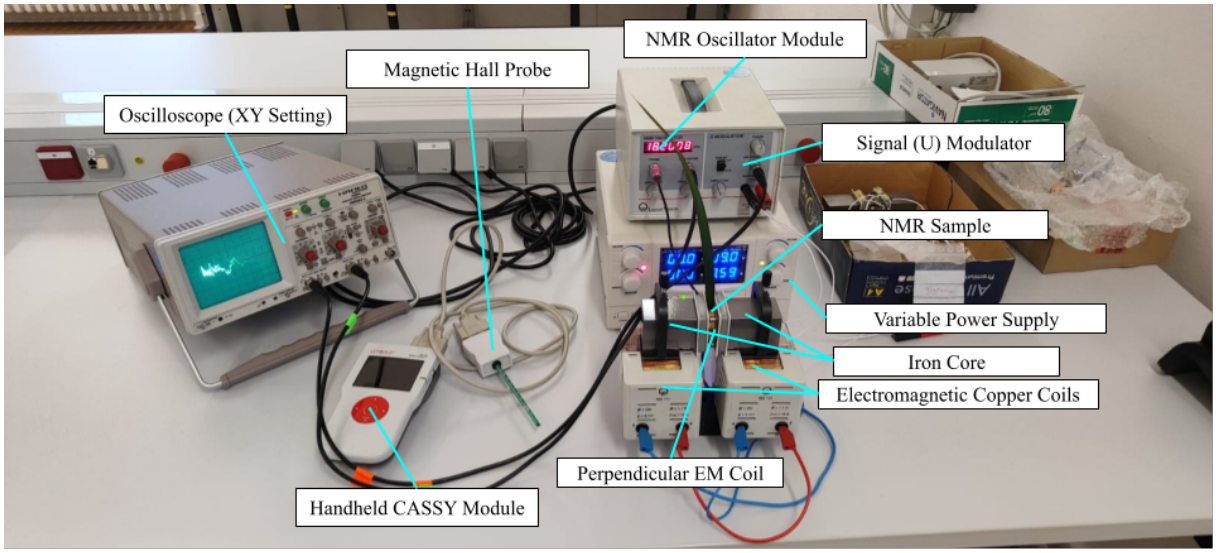

Figure 4: Annotated Setup Diagram for Nuclear Magnetic Resonance

After the Landé g-factor for DPPH was determined, and the corresponding half width magnetic field strength δB_0 and transition lifetime were determined in the Electron Spin Resonance experiment, the setup redesigned to examine the behavior of nuclear magnetic resonance. Similar to the electron spin resonance experiment, the NMR sample was placed in a small gap between an iron core which connects two large electromagnetic copper coils ran through a variable power supply. To change the magnetic field across the NMR sample, one simply changes the current through the use of variable power supply, and measures the magnetic field strength using a magnetic hall probe. As the sample is now placed between two halves of an iron core, the magnetic field across the NMR sample can be deemed much more uniform than the magnetic field across the ESR sample. For this reason, it is more reliable to use a magnetic Hall probe attached to a handheld CASSY unit to measure the magnetic field strength B_0 across the sample. To instate a variable magnetic field across the sample, a third coil is introduced around the NMR sample in a perpendicular direction. This coil is attached to an NMR Oscillator module capa-

ble of producing high frequencies in the MHz range. This module was connected to the input signal of the coupled oscilloscope (seen on the left), and the signal passed through the coil. As the apparatuses of this experiment were much closer together and fixed, less calibration of the instruments had to be performed in order to reach an optimal setup. The only calibration which was performed to ensure the quality of the measurements across all examined materials was the modification of the phase shift such that the two peaks lined up exactly. After the phase shift was calibrated for each material, the current across the electromagnet copper coils was varied in steps of approximately 0.1A from 3.1A to 3.6. A total of 5 measurements per medium were taken for an appropriate level of reliability of measurement. After these 5 resonant frequency measurements were taken with respect to the B-field, their relationship was plotted on a linear graph, the slope extracted, and then consequently applied to formula 2.23 to extract the g-factor of the examined medium. Using the theoretical values for the g-factor of various nuclei found in the compounds examined, it was possible then to identify the exact contributing nucleus which exhibited nuclear magnetic resonance through the simple comparison of the calculated g-factors to the theoretical ones. As the Magnetic field strength (B) could not be measured directly due to the highly calibrated Helmholtz coil setup, a theoretical prediction between the current across the Helmholtz coils and the magnetic field strength at the DPPH sample was used, specifically equation 2.20. By measuring the current through the use of the ammeter connected in series with the two parallel Helmholtz coils, the ammeter would read double the current across each Helmholtz coil. This is a direct effect of the fact that the two Helmholtz coils are connected in parallel, and therefore the current is split from what is measured across the ammeter.

4 Results and Data Analysis

To investigate the phenomenon of Electron Spin Resonance, the relationship between the resonant frequency ν and the static magnetic field strength (B), a DPPH element was subjected to an external magnetic field generated by Helmholtz coils which was further exposed to an orthogonally incident high frequency magnetic field B_{HF}. By using the oscilloscope to identify frequencies which yielded a uniform peak in voltage, the resonant frequencies of the DPPH element for different static external magnetic fields B were examined. In the first component of the investigation, the Landé g-factor was calculated after examining the relationship between resonant frequency and the external magnetic field. In order to do so, the necessary constants were measured such that accurate results could be obtained. To begin, the number of wrappings on each Helmholtz coil n was determined to be 320, and the radius of each was determined to be $0.068[m]$ to exact precision as provided by the producer.

$$n = 320 \quad \wedge \quad r = 0.068 \quad \text{(Materny \& Mohaghegh, 2025)} \tag{4.1}$$

Table 1: Relationship between Calculated Magnetic Field (from Current) and Frequency of AC B-Field		
Current I [A] ±0.001[A]	**Magnetic Field Strength B [T] ±4.24E-05[T]**	**Frequency [Hz] ± E+05[Hz]**
0.15	6.35E-04	1.54E+07
0.20	8.57E-04	2.00E+07
0.24	1.03E-03	2.52E+07
0.29	1.21E-03	3.01E+07
0.33	1.41E-03	3.50E+07
0.39	1.63E-03	4.00E+07
0.43	1.80E-03	4.50E+07
0.47	1.98E-03	4.99E+07
0.52	2.18E-03	5.51E+07
0.56	2.36E-03	6.00E+07
0.60	2.55E-03	6.51E+07
0.65	2.73E-03	7.00E+07
0.69	2.90E-03	7.51E+07
0.73	3.07E-03	8.00E+07
0.78	3.28E-03	8.49E+07
0.82	3.46E-03	9.01E+07
0.86	3.65E-03	9.50E+07
0.91	3.85E-03	1.00E+08
0.95	4.01E-03	1.05E+08
1.00	4.23E-03	1.10E+08
1.04	4.40E-03	1.15E+08
1.08	4.57E-03	1.20E+08
1.14	4.80E-03	1.25E+08

As the values of the number of wrappings and the radius are assumed to have zero absolute error, the only error which is present in our calculation of the magnetic field strength is the error propagated through equation 2.20 from the error in the current, I which is $\pm 0.01[A]$. Propagating this through equation 2.20, one achieves a minuscule value for the error of the magnetic field strength of $\approx \pm 4.23 \cdot 10^{-5}$ The table above represents a clear correlation between the frequency of resonance ν and the applied magnetic field strength B_0. The blue, red and green rows represent measurements taken with the large, medium and small coils respectively.

The table above tabulates all measurements relating the calculated magnetic field strength B–using equation 2.20–with the resonant frequency ν for the DPPH sample. By constructing a linear relationship between these two quantities and extracting their relative rate of change, the Landé g-factor can be easily determined through a simple rearrangement of the slope in equation 2.16. Using only the numerical results from the table, it is already clear that a strong positive relationship exists between the Magnetic Field Strength and the Resonant Frequency. Furthermore, it is important to note that the error of the calculated magnetic field strength and the resonant frequency are much smaller in comparison to the measurements taken, and therefore are likely not to show up visibly when converted to error bars. With the results tabulated, they were consequently plotted and fitted using a least squares regression, furthermore taking into account the absolute errors of the measurements in the form of error bars–so small they are barely visible on the plot. This visualization can be seen below in figure 5.

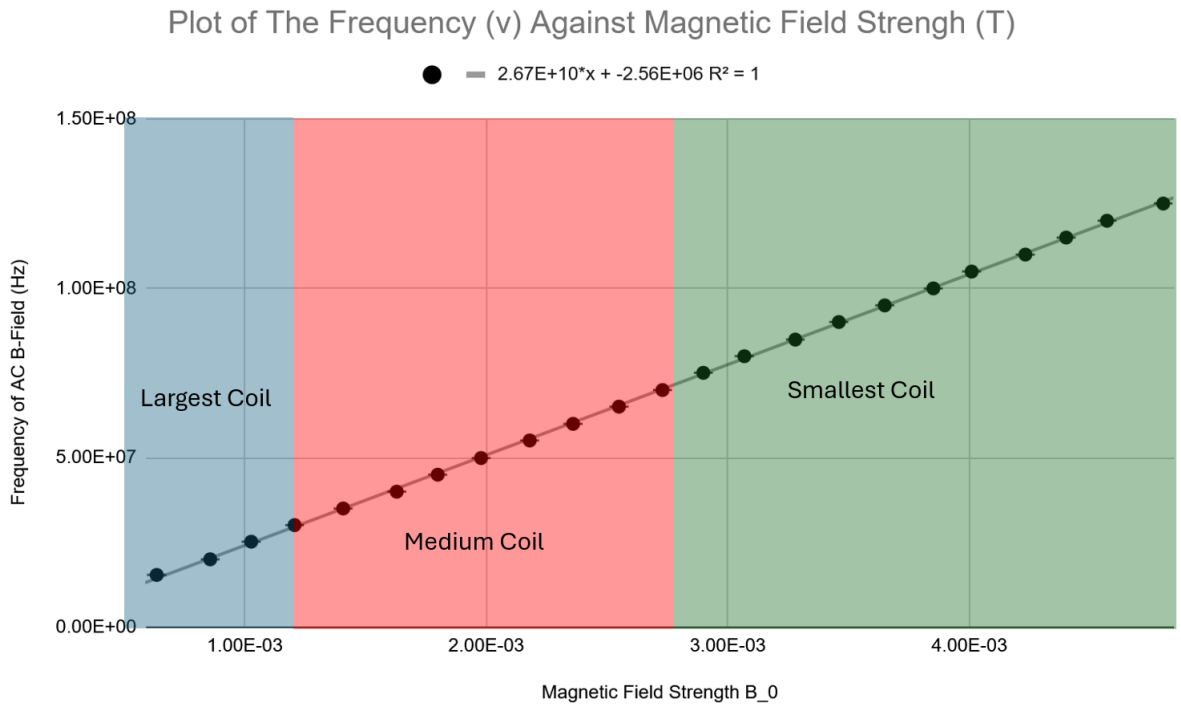

Figure 5: Plot of The Frequency (ν) Against Magnetic Field Strengh (T)

As predicted by the relevant theory, a clearly directly proportional relationship between the magnetic field strength and the frequency of the alternating orthogonal magnetic field is observed, and can be seen in figure 5 respectively. The graph is also color coded to easily relate the data in the table to the data on the graph, and to demonstrate domains of measurement corresponding to each secondary ESR coil used around the DPPH sample, indicated and labeled by the blue, red and green regions respectively. The slope of the graph was obtained to be $m = (2.67 \pm 0.008) \cdot 10^7 [HzT^{-1}]$, and the fit of the regression was accurate to an R^2 value of 1, which is the highest possible precision of correlation. This slope is directly related to the Landé g-factor through equation 2.16. Extracting only the slope of the equation and rearranging it to solve for the Landé g-factor, one achieves:

$$g_J = \frac{slope \cdot h}{\mu_B} \tag{4.2}$$

From this equation the Landé g-factor of the DPPH element was calculated to be:

$$g_J = 1.91 \pm 0.0059 \tag{4.3}$$

where the error in the measurement comes only from the error of the slope $\approx 0.8 \cdot 10^5 [HzT^{-1}]$, and is scaled directly by h and the Bohr magneton μ_B.

The literature value of the Landé g-factor for an electron in DPPH is expected to be around 2.0023, so our result agrees with the expected statistical value to a commensurable degree. Restating the theory that causes the Landé g-factor to be close to 2, one can look towards the molecular structure of the material, and the nature of its free radical. Due to the structure of the material, the orbital motion of the electron is nearly completely mitigated, leaving the g-factor close to that of a free electron (Materny & Mohaghegh, 2025). The calculated value is slightly lower than the expected value, but it remains within an statistically acceptable range as its percentage deviation is just under 5% at 4.83%. With the Landé g-factor calculated, the next significant values one can calculate are the half width of the magnetic field strength δB and the transition state lifetime T. To do so, we look to the phenomena exhibited in relation to the absorbed energy.

Since the absorbed energy is directly related to the voltage observed on the oscilloscope, an associated uncertainty was assigned to the measured voltage and the lifetime of the transition state for different frequencies was calculated. First of all, to determine δU, visual methods were employed to calculate the full-width at half maximum (FWHM) of the voltage curves using the Desmos graphing software. The peak signal value was identified through visual analysis and halved. The two points on the voltage curve with a voltage half of the maximum were taken, and the distance between them measured, as visually shown in figure 3. These measurements were taken for 3 different currents–and consequently resonant frequencies–allowing for the calculation of δI (using Equation 2.19) the corresponding uncertainties in the B-field (using Equation 2.20) and the transition state lifetime (using Equation 2.21). The calculated data for the half-width δB and the spin state lifetime T are presented in the table below for three different resonant frequencies.

Table 2:Calculated Data Table for δI, δB and lifetime T

Frequency [Hz]	$U_{mod}[V] \pm 0.25[V]$	$I_{mod}[A]$	$\delta[V] \pm 0.1[V]$	$\delta I[A]$	$\delta I\ Error[A]$	$\delta B[T]$	$\delta B Error[T]$	Lifetime T [S]	Lifetime Error [S]
5.00E+07	3	0.25	0.70	0.06	9.65E-03	2.47E-04	4.08E-05	1.21E-08	2.00E-09
4.00E+07	3	0.26	0.66	0.06	9.70E-03	2.37E-04	4.11E-05	1.26E-08	2.17E-09
6.00E+07	3	0.26	0.61	0.05	9.54E-03	2.19E-04	4.03E-05	1.36E-08	2.50E-09

As three separate values were calculated for the transition state lifetime, the best estimate is obtained by taking the arithmetic mean of all three values. In doing so, a more accurate and less error prone value for the lifetime will be obtained. Averaging across all transition state lifetimes T as calculated using formula 2.21, the average transition state lifetime T across all measured resonant frequencies ν was calculated to be:

$$T = (1.27 \pm 0.222) \cdot 10^{-8}[s] \tag{4.4}$$

where the error was calculated through the propagation of formula 2.21. And the corresponding instrumental errors of variables present in the equation.

Furthermore, the three widths of the magnetic field strength curve were calculated using formula 2.20 for each of the three frequencies 50MHz, 60MHz, 70MHz respectively as:

$$\delta B_{50} = (2.47 \pm 0.4) \cdot 10^{-4}[T] \tag{4.5}$$

$$\delta B_{60} = (2.37 \pm 0.4) \cdot 10^{-4}[T] \tag{4.6}$$

$$\delta B_{70} = (2.19 \pm 0.4) \cdot 10^{-4}[T] \tag{4.7}$$

In order to successfully investigate the phenomenon of Nuclear Magnetic Resonance (NMR), 4 different samples–Glycerin ($C_3H_8O_3$), Teflon (PTFE, C_2F_4), Polystyrene (C_8H_8) and plant matter (composition not directly known)– were subject to a constant magnetic field B_0 and a high frequency alternating orthogonal B-field. Exactly the same as the method used to calculate the Landé g-factor during the electron spin resonance experiment, the relationship between the resonant frequency ν of the organic material and the static magnetic field strength B_0 across the sample will be measured and the g-factor of the material extracted. Using the calculated g-factor, it is then possible to determine the major contributing nuclei and the free radical. The g-factor of a material is determined directly by its gyromagnetic index γ, which is specifically the ratio of its magnetic moment μ to its angular momentum $|\vec{J}|$ (AD, 2024).

$$g = \frac{2m_p}{\gamma} \tag{4.8}$$

In order to best compare the calculated g-factors to literature, it is necessary to first tabulate the necessary elements and their corresponding g-factors into a table. As the elements of the organic molecules used during this experiment are Oxygen, Hydrogen, Carbon, and Fluorine, their g-factors will be put into a table for reference and for the later analysis of the calculated g-factors.

Table 3: Theoretical Values with Gyromagnetic Ratio and g-factor for Relevant Elements

Element	Elementary Charge	Mass of Proton	Gyromagnetic Ratio	g-factor
Hydrogen-1	1.60E-19	1.67E-27	2.68E+08	5.59
Carbon-13	1.60E-19	1.67E-27	6.73E+07	1.41
Fluorine-19	1.60E-19	1.67E-27	2.52E+08	5.26
Oxygen-17	1.60E-19	1.67E-27	-3.63E+07	-0.76

Table 3 demonstrates the theoretical values of the gyromagnetic ratio and corresponding g-factor for Hydrogen-1, Carbon-13, Fluorine-19, and Oxygen-17. These 4 materials are those that are present within the elements to be investigated using nuclear magnetic resonance, and the theoretical g-factors are statistically given as:

$$g_H = 5.59 \quad \text{(Bellis, 2024)} \tag{4.9}$$

$$g_C = 1.41 \quad \text{(Bellis, 2024)} \tag{4.10}$$

$$g_F = 5.26 \quad \text{(Bellis, 2024)} \tag{4.11}$$

$$g_O = -0.76 \quad \text{(Jaeck, 2024)} \tag{4.12}$$

As one can see from the theoretical values above, the nucleus with the largest g-factor is Hydrogen-1, likely due to its extreme dipole like structure. The smallest of the g-factors used for this experiment is that of Oxygen-17, which has a negative g-factor. This negative g-factor is likely due to the configuration of its unpaired nucleon and the nature of nuclear interactions. Specifically, Oxygen-17 has 17 neutrons and only 16 protons, which means that the is 1 unpaired neutron. This unpaired neutron sits in the $1d_{5/2}$ orbital, giving the element a negative magnetic moment, and therefore a negative gyromagnetic ratio γ and g-factor. By comparing the calculated g-factors for each organic molecule and and the corresponding theoretical values, the major contributing nuclei and the free radical can be determined. To begin, the nuclear magnetic resonant properties of Glycerin ($C_3H_8O_3$) were measured by taking 5 measurements of the resonant frequency with respect to the magnetic field strength across the sample (measured using a magnetic hall probe). Table 4 tabulates the collected data.

Table 4: Measured Values of Resonant Frequency against Magnetic Field Strength for Glycerin ($C_3H_8O_3$)

Current $\pm 0.01[A]$	Magnetic Field Strength $\pm 0.001[T]$	Resonant Frequency $\pm 10^2[Hz]$
3.1	0.421	1.75E+07
3.2	0.429	1.79E+07
3.31	0.434	1.84E+07
3.48	0.441	1.82E+07
3.57	0.457	1.91E+07

From only the table, it is clear that a strong positive relationship exists, as the current increases, the magnetic field strength increases proportionally, thereby inducing an increase in the resonant frequency of the target nucleus. Note that the currents were only ranged from $3.1[A]$ to $3.6[A]$ in order to keep the resonant frequency in a reasonable range which is possible for the NMR unit to reach. In this particular measurement series, a maximum of $\approx 19[MHz]$ was reached. To better extract the rate of change of the resonant frequency with respect to the change in magnetic field, a plot of the frequency against magnetic field strength for Glycerin is made. Using the slope, one can calculate the associated g-factor by applying formula 2.23. Below is the graph of the data presented in Table 4.

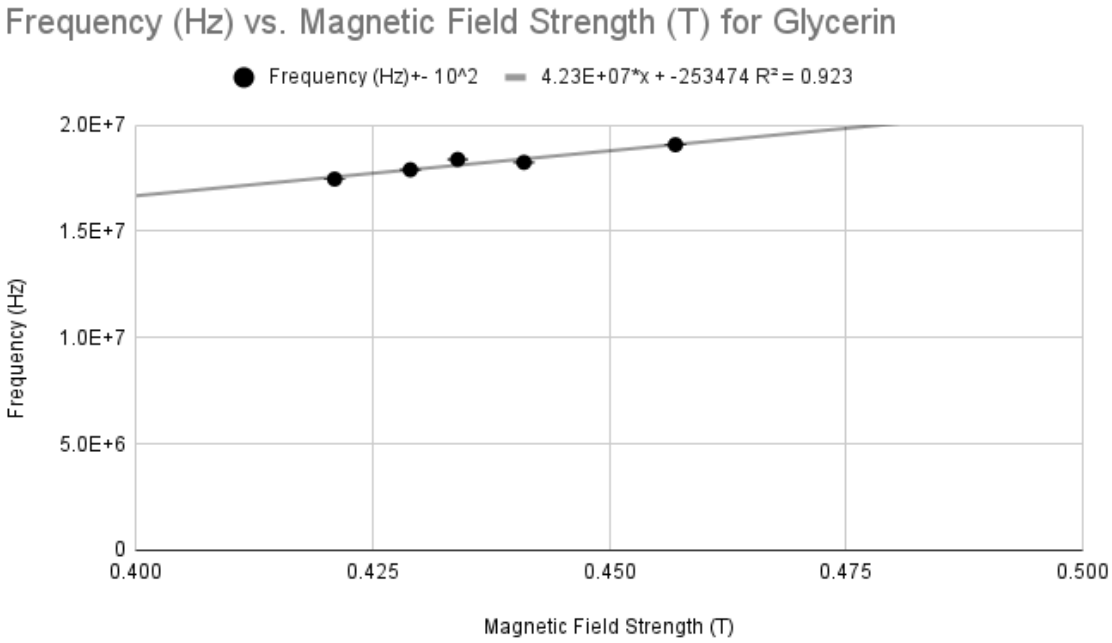

Figure 6: Frequency (Hz) vs. Magnetic Field Strength (T) for Glycerin

In the graph above, one can see an approximate positive linear correlation between the Magnetic Field Strength across the Glycerin sample and the resonant frequency. Note that the graph does indeed contain error bars, however due to their size, are nearly invisible on the plot. This is due to the uncertainty of the resonant frequency only lying at around 100Hz, while measurements are taken in the MHz range. This is simply an indication of very precise measurements. As one can observe from the plots, a semi-accurate fit is obtained with an R^2 value of 0.923. Additionally, the extracted slope of the relationship between the frequency and the magnetic field strength is given as:

$$\nu = (4.23 \cdot 10^7)B_0 + 253474 \tag{4.13}$$

Substituting this slope $\approx (4.23 \pm 0.7) \cdot 10^7[HzT^{-1}]$ into formula 2.23, one obtains a final g-factor for Glycerin ($C_3H_8O_3$) of:

$$g_{j_{\text{glycerin}}} = 5.56 \pm 0.93 \tag{4.14}$$

While our g-factor has quite a high propagated error, the closest theoretical g-factor to that of Glycerin is **Hydrogen-1**, which has a g-factor of 5.59, our estimate only 0.03 off. This may be made sense of by the molar abundance of hydrogen in the Glycerin ($C_3H_8O_3$) molecule. Moving forward, the nuclear magnetic properties of Polystyrene (C_8H_8) were measured, and the g-factor determined in a similar manner. The tabulated values of the magnetic field strengths (due to currents between 3.1A and 3.6A) and the observed resonant frequency can be seen in Table 5 below.

Table 5: Measured Values of Resonant Frequency against Magnetic Field Strength for Polystyrene (C_8H_8)		
Current $\pm 0.01[A]$	Magnetic Field Strength $\pm 0.001[T]$	Resonant Frequency $\pm 10^2[Hz]$
3.11	0.408	1.79E+07
3.22	0.411	1.80E+07
3.3	0.421	1.83E+07
3.41	0.429	1.87E+07
3.55	0.438	1.91E+07

As observed in the table above, there is once again a positive relationship observed between the magnetic field strength B_0 across the sample and the resonant frequency ν. To better visualize this data, the measurements are plotted again such that the relationship between Resonant Frequency and Magnetic Field Strength can be analyzed. Below is the respective plot.

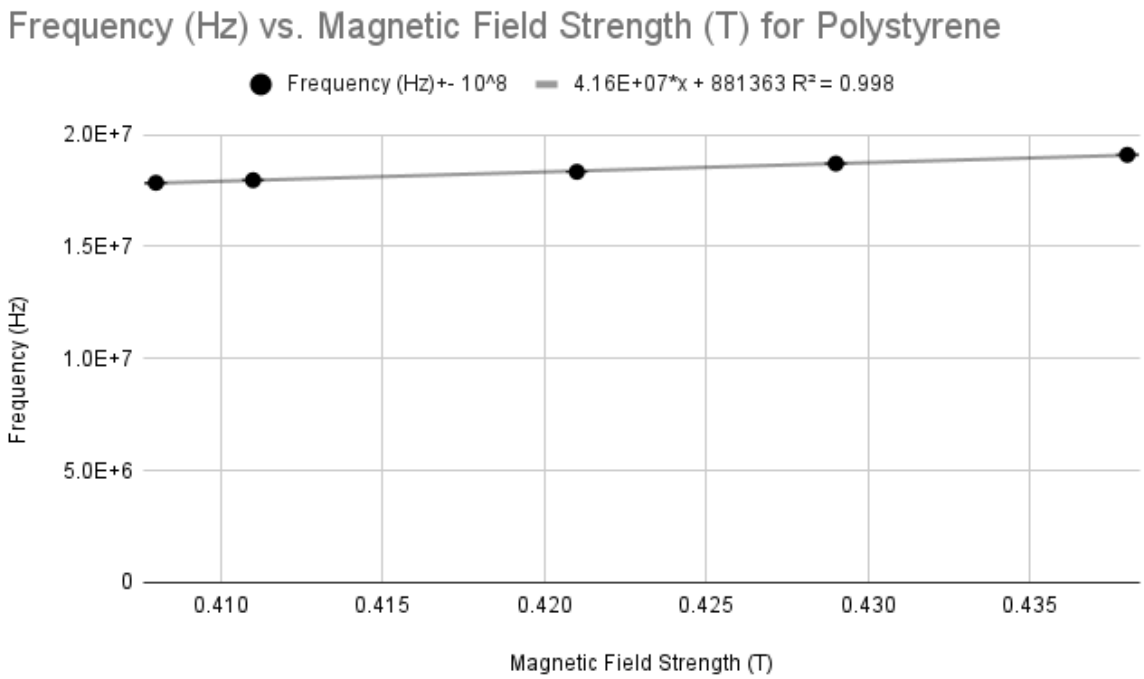

Figure 7: Frequency (Hz) vs. Magnetic Field Strength (T) for Polystyrene

Quite similar to Glycerin, Polystyrene exhibits a positive relationship between the Frequency and Magnetic Field strength, indicating immediately a positive g-factor. It is also important to note that the quality of this linear regression fit is much higher than that of Glycerin, with an R^2 value of 0.998. To explicitly calculate this g-factor, the slope of the graph, $(4.17 \pm 0.09) \cdot 10^7[HzT^{-1}]$ is substituted into equation 2.23, yielding a final g-factor for Polystyrene of:

$$g_{j_{\text{Polystyrene}}} = 5.46 \pm 0.13 \tag{4.15}$$

Immediately, one can see that the uncertainty of the g-factor for Polystyrene is much less than that of Glycerin, indicating a better precision of measurement. Comparing the g-factor of Polystyrene to that of the theoretical values, it most closely matches with **Hydrogen-1**, very similarly to Glycerin. This makes sense as both materials contain Hydrogen-1 as an isotope, so they would share certain similarities in this matter. Up to this point, all molecules subject to examination under nuclear magnetic resonance (NMR) have had Hydrogen. The next material to be analyzed is PTFE, commonly known as Teflon is an organic fluorocarbon (C_2F_4) solid, meaning that it contains no Hydrogen. To calculate its g-factor it was again subject to a variable magnetic field and its frequency change analyzed. Table 6 below tabulates the data collected for PTFE.

Table 6: Measured Values of Resonant Frequency against Magnetic Field Strength for PTFE (C_2F_4)		
Current $\pm 0.01[A]$	Magnetic Field Strength $\pm 0.001[T]$	Frequency $\pm 10^2[Hz]$
3.10	0.41	1.64E+07
3.25	0.43	1.70E+07
3.42	0.44	1.75E+07
3.52	0.45	1.78E+07
3.59	0.45	1.81E+07

Again, the table shows a strong positive correlation, however this time the maximum resonant frequency achieved is less than that of both Glycerin and Polystyrene, $\approx 1.89 \cdot 10^7[Hz]$. To verify that this is indeed the case and has an effect on the calculated g-factor, the data is again visualized in a plot below.

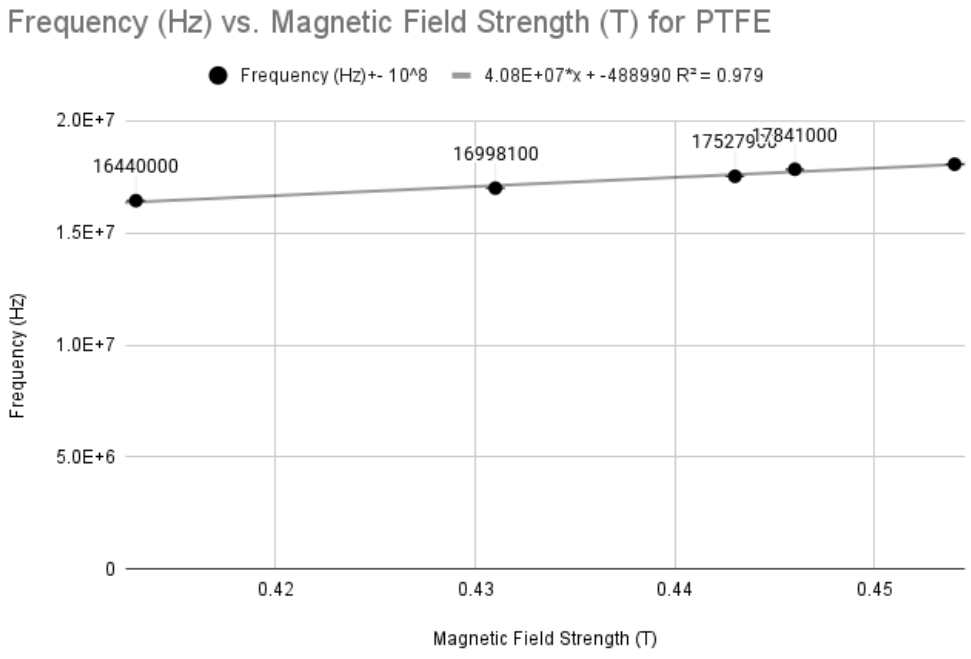

Figure 8: Frequency (Hz) vs. Magnetic Field Strength (T) for PTFE (Teflon)

Table 7: Measured Values of Resonant Frequency against Magnetic Field Strength for Plant (Chemical Structure Unknown)		
Current $\pm 0.01[A]$	Magnetic Field Strength $\pm 0.001[T]$	Frequency $\pm 100[Hz]$
3.10	0.391	1.70E+07
3.14	0.408	1.77E+07
3.29	0.421	1.82E+07
3.50	0.430	1.90E+07
3.61	0.446	1.93E+07

As predicted from the table, it is clear that the slope of the relationship between the frequency and magnetic field strength is indeed small than that of Glycerin and Polystyrene. While the fit of the graph is commensurable with an R^2 value of 0.979, there are small deviations. It is also important to note that error bars are indeed included, however due to the scaling of said error bars are near impossible to discern. As the slope of the graph for PTFE is given by $\approx (4.08 \pm 0.383) \cdot 10^7 [HzT^{-1}]$, one can calculate the g-factor of Teflon to be:

$$g_{j_{\text{Teflon}}} = 5.36 \pm 0.5 \tag{4.16}$$

This result falls directly in range of the g-factor for **Fluorine-19**.

As a further investigation into living organic materials and more complex unknown structures, the chemical composition and major contributing nuclei of a plant sample was examined. In order to do so, a plant leaf was picked and crushed such that it fit into a sample container. This container was then placed into the sample space as normal, and an NMR analysis was conducted in the same way. Below is the tabulated data of the Plant Sample relationship between resonant frequency and magnetic field strength across the sample.

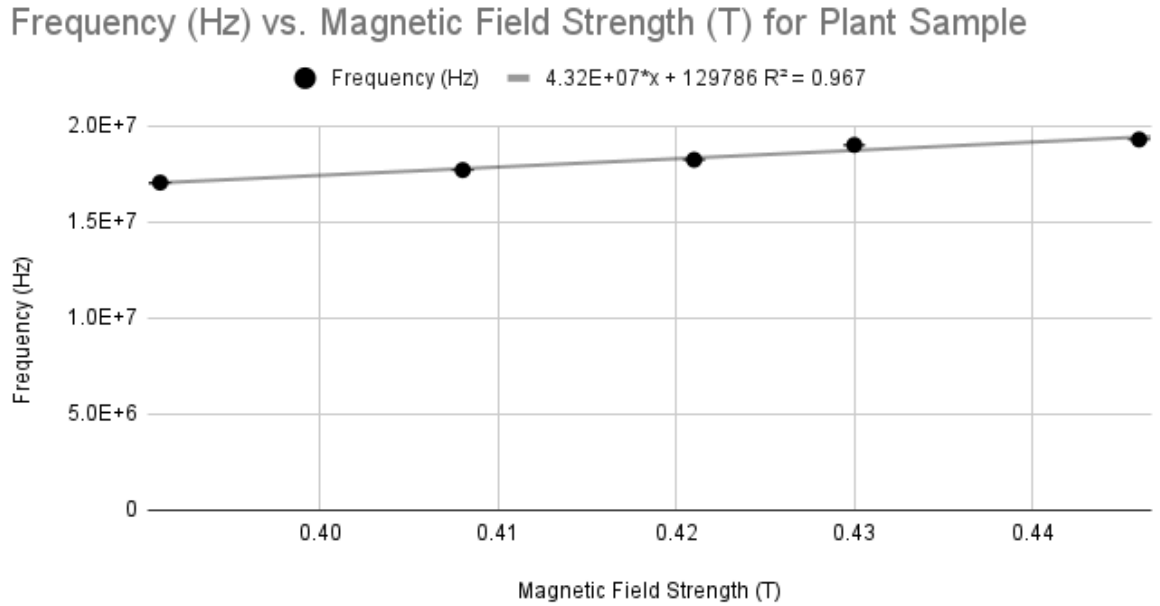

Figure 9: Frequency (Hz) vs. Magnetic Field Strength (T) for Plant Sample

From the table alone, quite a strong postive correlation is present, similar to that of Glycerin and Polystyrene. This leads one to believe that the main constituent of the plant responsible for nuclear magnetic resonance behavior is hydrogen. To ensure that this is indeed the case, the tabulated values in Table 7 were plotted, and the slope extracted. Above is the plot of the resonant frequency ν for a plant sample against its incident static magnetic field strength B_0. As one can see from the plot, a strong positive correlation between the two measurements indeed exists, and with a slope of $\approx (4.32 \pm 0.5) \cdot 10^7 [HzT^{-1}]$. The correlation coefficient R^2 of the regression is also quite good considering the impurity of the sample taken, and is given as ≈ 0.967. Substituting the slope into equation 2.23, one achieves a final value for the g-factor of the plant sample of:

$$g_{j_{\text{Plant}}} = 5.68 \pm 0.5 \tag{4.17}$$

This g-factor is the highest out of all g-factors calculated throughout this investigation, and corresponds most closely to the nucleus of **Hydrogen-1**. This makes quite a bit of sense as many living organisms, specifically flora, are built up from Hydrogen, Carbon, and Oxygen.

5 Error Analysis

For all errors involving the slope of the graph, the uncertainty of the slope was approximated using the built-in function (LINEST), which works by approximating the linear slope of a set of data points through the least squares method. As a byproduct, the error of the slope is given in absolute form. Due to the efficiency of this method, and the large quantity of graphs, it was the clear choice for this investigation.

For all errors involving numerical calculations with propagated error, such as for the uncertainties of the final measurements of the Kerr Constant and Verdet Constants, the root sum of squares method (RSS) was employed. This method involves calculating the propagated error of a formulaic value by computing all partial derivatives with respect to all error-prone parameters, and taking it under a square root. The formula for this is given below.

$$\Delta y = \sqrt{\sum_{i=0}^{n} \left(\frac{\partial y}{\partial x_i} \cdot \Delta x_i \right)^2} = \sqrt{\left(\frac{\partial y}{\partial x_1} \cdot \Delta x_1 \right)^2 + \cdots + \left(\frac{\partial y}{\partial x_n} \cdot \Delta x_n \right)^2} \tag{5.1}$$

For the ESR experiment, the magnetic field strength was determined using the current through the Helmholtz coils. Since the permeability of free space, the number of coil turns, and the coil radius are constants, the primary source of error arises from the uncertainty in the current measurement. The absolute uncertainty in B was found using error propagation:

$$\Delta B = \mu_0 (\frac{4}{5})^{\frac{3}{2}} \frac{n}{r} \Delta I \tag{5.2}$$

with an uncertainty of $\Delta I = 0.01A$ (instrumental error). The frequency measurements were taken directly from the oscilloscope with an instrumental error of$\pm 10^5$.

The Landé g-factor was derived from the slope of the frequency versus magnetic field plot equation 4.2. Where the error of the slope was found using LINEST function. The uncertainty of g_J was obtained via error propagation. Errors in this experiment could arise from systematic inaccuracies in the magnetic field calibration, frequency measurement, and environmental factors such as temperature fluctuations or electromagnetic interference. Also from not aligning the coils perfectly parallel. These could lead to deviations in resonance.

$$\Delta g_J = \frac{h}{\mu_B} \Delta slope \tag{5.3}$$

In the NMR experiment, the half-width δB was determined from the resonance curves using Full Width at Half Maximum (FWHM) methods. The instrumental errors of $\Delta U_{mod}\ and\ \Delta I_{mod}$ were $\pm 0.25\ and\ 0.0005$, respectively. (Error for the I_{mod} was halfed since initially $2I_{mod}$ was measured. The error of the δU was measured to be 0.1 caused by oscilloscope resolution in voltage measurements. Using the measured values and equation 2.19, δI was calculated with the corresponding uncertainty:

$$\Delta_{\delta I} = \delta I \cdot \sqrt{\left(\frac{\Delta(\delta U)}{\delta U}\right)^2 + \left(\frac{\Delta I_{\text{mod}}}{I_{\text{mod}}}\right)^2 + \left(\frac{\Delta U_{\text{mod}}}{U_{\text{mod}}}\right)^2}$$

and error of the δB was calculated using the similar formula:

$$\Delta \delta B_0 = \mu_0 (\frac{4}{5})^{\frac{3}{2}} \frac{n}{r} \Delta \delta I \tag{5.4}$$

To calculate the error of the lifetime, the following formula was used:

$$\Delta T = T \cdot \sqrt{\left(\frac{\Delta g_J}{g_J}\right)^2 + \left(\frac{\Delta \delta B_0}{\delta B_0}\right)^2} \tag{5.5}$$

For the NMR experiment, the primary sources of error stemmed from uncertainties in magnetic field strength measurements, frequency detection, and the linear fit used to determine the g-factor. The magnetic field strength was measured using a B-probe. The possible uncertainties could be caused by: instrumental errors of the probe, fluctuations in the power supply current, and experimental alignment inconsistencies. Both the estimated magnetic field error of $\pm 0.001T$ and frequency measurements with the error of $\pm 100Hz$, influenced on the error of the g-factor. The errors of the slopes of the frequency vs. B_0 were obtained using the LINEST function. The uncertainty of the g-factor was calculated using the following formula:

$$\Delta g_{J_N} = \frac{h \cdot \Delta slope}{\mu_N} \tag{5.6}$$

Where μ_N is the nuclear magneton and h is the Planck constant, both of them are constant values with 0 uncertainty. Despite these sources of error, the obtained values were within reasonable agreement with theoretical predictions, validating the experimental setup and data collection methods.

6 Discussion

The results of the Electron Spin Resonance (ESR) and Nuclear Magnetic Resonance (NMR) experiments demonstrate a strong correlation between theoretical predictions and experimental observations. The linear relationships observed in both experiments between resonance frequency and magnetic field strength confirm the fundamental principles about the spin resonance phenomena. For the electron spin resonance (ESR), the calculation of the Landé g-factor for the DPPH sample yielded a value of 1.91 ± 0.0059, which is in reasonable agreement with the theoretical value of 2.0023 for a free electron. The small deviation from the expected value can be attributed to a combination of systematic and random errors. The half-width δB_0 is a crucial parameter, which influences the calculated transition lifetime T. The transition lifetime T was also successfully determined to be $T = (1.27 \pm 0.222) \cdot 10^{-8}$[s]. The observed value of δB across different frequencies showed minor variations. The precision of these measurements depended on the accuracy of voltage peak determination using the Full Width at Half Maximum (FWHM) method. Potential sources of error in determining δB_0 include uncertainties in oscilloscope resolution and noise in the signal. However, the consistency of the obtained values suggests that the methodology was effective in capturing the width accurately. Possible sources include imperfections in the alignment of the Helmholtz coils, minor fluctuations in the power supply and limitations in the oscilloscope resolution when determining frequency peaks. Random errors could also have arisen from variations in sample placement. However, the high precision of the measurement, and the low uncertainty of the g-factor, suggests that the setup and methodology were effective.

The NMR experiment focused on optimizing the signal and determining the nuclear g-factor of glycerin, PTFE (Teflon), and polystyrene by analyzing the resonance frequency as a function of magnetic field strength. The calculated g-factors for these materials were:

- Glycerin: $g_{J_{\text{Glycerin}}} = 5.56 \pm 0.93$, closely matching the theoretical g-factor of Hydrogen-1 ($g_H = 5.59$). This confirms that the dominant nuclei in glycerin is are hydrogen nuclei.
- Polystyrene: $g_{J_{\text{Polystyrene}}} = 5.46 \pm 0.13$, again this value aligns mostly with Hydrogen-1, which was expected given the presence of hydrogen in the structure.
- PTFE (Teflon):$g_{J_{\text{Teflon}}} = 5.36 \pm 0.5$, corresponds to Fluorine-19 ($g_F = 5.26$), which is dominant nucleus in PTFE.

The agreement between the experimental and theoretical values strongly supports the effectiveness of the method, and helps to identify the primary nuclei which are responsible for the NMR signals. However, some deviations such as in glycerin, are likely due to the inhomogeneities in the sample or due to the small fluctuations in the applied magnetic field. The additional analysis of a plant sample aimed to detect NMR signals from organic matter. The detected resonance frequencies and calculated g-factor suggested a dominant contribution from the hydrogen nuclei, which is expected because of the hight water content and molecular structure of the plants. However, it was harder for the plant sample to detect the peaks, indicating the influence of other elements as well. Further experiments using a broader range of external field or using higher resolution spectroscopy would be needed to fully characterize the plant tissue. Despite these challenges, the experimental results were largely consistent with theoretical expectations. The experiment demonstrated the ESR and NMR techniques and determined the fundamental magnetic properties of materials. Future improvements could include using higher-resolution instruments, automated data acquisition for increased precision, more precise sample positioning methods and more advanced calibration techniques to minimize systematic errors.

7 Conclusion

In this investigation, the phenomena of Electron Spin Resonance and Nuclear Magnetic resonance were successfully examined to a commendable degree. During the analysis of the Electron Spin Resonance, the Landé g-factor of a DPPH element subject to a very small magnetic field was determined, and the half width of the magnetic field δB alongside the transition state lifetime T. When analyzing the final results of this experiment, it is important to note the technical difficulty that this setup brings in comparison to traditional methods of ESR and NMR. While in traditional ESR schemes a magnetic field density of near 1T is used across the sample, the experiment conducted during this investigation only made use of incident magnetic field strengths on the mT scale, the reason this is possible due to the nature of the DPPH element examined. For the ESR experiment, the calculated values of experimental interest were the Landé g-factor g_J, the magnetic field density signal width δB and the transition state lifetime T:

$$g_J = 1.91 \pm 0.0059 \tag{7.1}$$

$$\delta B_{50MHz} = (2.47 \pm 0.4) \cdot 10^{-4}[T] \tag{7.2}$$

$$\delta B_{60MHz} = (2.37 \pm 0.4) \cdot 10^{-4}[T] \tag{7.3}$$

$$\delta B_{70MHz} = (2.19 \pm 0.4) \cdot 10^{-4}[T] \tag{7.4}$$

$$T = (1.27 \pm 0.222) \cdot 10^{-8}[s] \tag{7.5}$$

The value obtained for the Landé g-factor coincides with the relevant theory to a commensurable degree. Furthermore, the values of the magnetic field density width δB exhibit a clear negative trend with respect to the resonant frequency, indicating that the width of magnetic field densities with higher resonant frequencies are more concentrated. Lastly, the averaged value of the transition state lifetime T is additionally in agreement with values compared with others who have completed this same derivation. For the NMR experiment, the calculated values of the g-factor very appropriately highlighted the NMR dominant contributions from each of the materials: Glycerin, Polystyrene, PTFE, and Plant Matter.

$$g_{J_{\text{Glycerin}}} = 5.56 \pm 0.93 \tag{7.6}$$

$$g_{J_{\text{Polystyrene}}} = 5.46 \pm 0.13 \tag{7.7}$$

$$g_{J_{\text{Teflon}}} = 5.36 \pm 0.5 \tag{7.8}$$

$$g_{j_{\text{Plant}}} = 5.68 \pm 0.5 \tag{7.9}$$

These values compare very nicely to the theoretical values and immediately indicate the dominating contributor the NMR behavior. For Glycerin, this contributor was Hydrogen-1, for Polystyrene Hydrogen-1 as well, Teflon was Fluorine-19, and for the Plant was Hydrogen-1.

---

8 Bibliography

References

AD, E. (2024). *Gyromagnetic ratio*. https://mriquestions.com/gyromagnetic-ratio-gamma.html. ELSTER LLC.

Bellis. (2024). *Nmr properties of commonly studied isotopes*. https://www.acadiau.ca/~bellis/resources/index.html. Acadiau.

Jaeck, A. (2024). *Properties and data of the isotope 17o*. https://www.chemlin.org/isotope/oxygen-17. Chemlin.

Materny, P. D. A., & Mohaghegh, D. F. (2025). Advanced physics lab ii manual. *Constructor University*.